Original Article
Effect of local application of biphosphonates on improving peri-implant osseointegration in type-2 diabetic osteoporosis

Xiaoqian Ding[1,2,3], Lan Yang[1,2,3,4], Yun Hu[1,2,3], Jinfeng Yu[1,2,3,5], Yu Tang[1,2,3], Dan Luo[1,2,3], Leilei Zheng[1,2,3]

[1]College of Stomatology, Chongqing Medical University, Chongqing 401147, China; [2]Laboratory of Medical Biochemistry, Chongqing Key Laboratory of Oral Diseases and Biomedical Sciences, Chongqing 401147, China; [3]Laboratory of Medical Biochemistry, Chongqing Municipal Key Laboratory of Oral Biomedical Engineering of Higher Education, Chongqing 401147, China; [4]Department of General Hospital, People's Hospital of Rongchang District, Chongqing 402460, China; [5]Department of Orthodontics, Haishu District Stomatology Hospital, Ningbo 315000, Zhejiang, China

Abstract: Type 2 diabetes mellitus (T2DM), a leading cause of osteoporosis, remains a contraindication for bone implant therapy. Although associated with side effects when systemically administered, biphosphonates (BPs) play a positive role in diabetic osteoporosis treatment. We hypothesized that local BP therapy would prevent decayed implant osseointegration under T2DM conditions. To assess cell proliferation and determine the optimal BP concentration, bone marrow-derived mesenchymal stem cells (BMSCs) and bone marrow macrophages (BMMs) were treated with BPs at various relatively low concentrations (10^{-9} mmol/L) for different periods of time. Our in vitro study results demonstrated that BP application reversed the process by which high glucose inhibits bone formation and stimulates bone resorption through osteoclast-specific gene and protein expression (P<0.05). In vivo, fat accumulation and insulin resistance were induced in T2DM rats. We used crosslinked hyaluronic acid as the drug delivery vehicle for BPs to ensure that BPs administered at a dose of 30 μg/kg could settle into the prepared hole in rats. Thereafter, implants were inserted into cylindrical holes of a specific size, created parallel to the long axis of the femora. The outcomes of the in vivo study revealed that BPs promoted bone formation, which reversed the reduction in the DM group according to double fluorescence labeling, micro-CT, biomechanical and histomorphometric analyses (P<0.05). Furthermore, intergroup comparisons revealed significant correlation coefficients (P<0.05) between the micro-CT and biomechanical parameters. Therefore, local administration of BPs could stimulation bone remodeling and represent an effective treatment strategy for preventing decayed implant osseointegration under T2DM conditions.

Keywords: Osteoporosis, type 2 diabetes mellitus, implant, bisphosphonates, osseointegration

Introduction

Osteoporosis is a major public health concern worldwide that involves deleterious performance of bone minerals and consequently enhances the danger of fracture. Various factors have been proven to be dangerous in osteoporosis, including estrogen deficiency, advanced age, and female sex [1]. Accumulating evidence has shown that patients suffering from type 2 diabetes mellitus (T2DM) have an increased risk of osteoporotic fractures and reduced bone formation [2-5]. The incidence of

T2DM and osteoporosis increases with aging of the population [6]. The mechanisms underlying the increase in bone fragility in patients with T2DM are, however, still not completely understood. To achieve successful implantation surgery with long-lasting outcomes, especially in patients who suffer the worst symptoms, such as inferior bone quality, strong, direct contact between the surfaces of the bone and the implant is required [7, 8]. Considering the aim of a successful bone implantation procedure, osseointegration is currently defined as direct interaction between the surfaces of the bone

and the implant. Accordingly, diabetes, a high-risk condition for implant treatment, often leads to delayed healing, premature loss of the implant, infection or osseointegration defects [9]. Many therapeutic agents have been found to increase the success rate of implant osseo-integration in osteopenic bone [10].

Numerous experimental approaches have been investigated to accelerate the maturation and regeneration of bone, shorten the therapeutic process, promote quality, and reduce the risk of nonunion. For these objectives, additional modalities, such as growth factors, hormones, calcium sulphate, and electrical stimulation, have been used [11-13]. Bisphosphonates (BPs), effective inhibitors of bone resorption, are considered the first-line treatment for osteoporosis and other bone diseases, such as multiple myeloma and malignant hypercalce-mia [14]. Nonetheless, the mechanism of how BPs act on osteoblasts and osteoclasts remains unclear, despite many years of investigation. However, clinical signs of complications related to systemically administered BPs, such as emesis, nausea and abdominal pain, have been observed in previous studies [15]. More-over, osteonecrosis and other side effects could be caused in some cases by systemic long-term and high-dose administration of BPs [16]. The optimal therapeutic period and the effect on decreasing the risks related to long-term, systemic exposure of BPs remain to be elucidated [17]. To prevent side effects due to systemically administered BPs, recent investigations have revealed modes of local delivery as viable replacement strategies [18], either by directly spreading BPs on the operative site before implant insertion or by delivering BPs to the surface of the implant [19, 20]. Additionally, local treatment protocols appears to be effective [21]. Although many related studies have been reported, most studies are limited to in vitro or in vivo experiments [21-24]. It remains uncertain whether local administration of BPs can mitigate bone resorption and promote implant osseointegration after the pathogenesis of diabetic osteoporosis.

We hypothesized that local administration of BPs could prevent decayed implant osseointegration under T2DM conditions. The present study aimed to assess in vivo and in vitro the effects of local administration of BPs in strepto-zotocin-induced rats with T2DM and the effects on relative cells under high glucose conditions.

Materials and methods

Biological characterization in vitro

Cell culture and differentiation: The animal research was approved by the local committee for Animal Care and Ethics. Sprague Dawley (SD) rats were purchased from Chongqing Medical University (Chongqing, China). Sub-sequently, bone marrow-derived mesenchymal stem cells (BMSCs) were cultured and identi-fied in accordance with a method previously described by our research group [25]. The dif-ferentiation of BMSCs was confirmed by osteo-genesis and adipogenesis. Cells were seeded in 12-well plates ($4*10^4$ cells/well) and cultured in osteogenic medium (OIM, normal glucose: 5.5 mmol/L) supplemented with ascorbic acid, dexamethasone and β-glycerolphosphate at 37°C with 5% CO_2 at 3 weeks. The medium was replaced every 2-3 days. After maintaining in culture for 3 weeks, cells were harvested, fixed with 4% paraformaldehyde for 30 min at room temperature, washed three times with PBS solution and then stained with 0.1% Alizarin red-S (Solarbio, China) for 30 min to detect min-eralized extracellular matrix. The formation of calcium nodules was assessed by a micro-scope (Nikon, Japan) [26].

Bone marrow macrophages (BMMs) were extracted from mouse femurs and tibiae, incu-bated, and cultured in α-MEM (Gibco) contain-ing 10% fetal bovine serum (FBS; Gibco) at 37°C with 5% CO_2 supplemented with 30 ng/mL macrophage colony stimulating factor (M-CSF; R&D Systems) to force them to differenti-ate into BMMs, as osteoclast precursors, which were seeded in 24-well plates ($1*10^4$ cells/well). After incubation under the abovemen-tioned conditions for 12 h, the cells were well attached to the dish and supplemented with 50 ng/ml recombinant mouse receptor activator of nuclear factor-κB ligand (RANKL; R&D Systems) and 30 ng/ml M-CSF. The culture medium was replaced every day. Mature osteoclasts that manifested as large and multinucleated cells formed after 6 days of culture [27].

Cell proliferation and cytotoxicity analysis

Cell proliferation was detected by a Cell Counting Assay Kit-8 (CCK-8; Tongren, Japan) according to the manufacturer's instructions. Primary BMSCs were cultured in 96-well plates ($1*10^3$ cells/well) and exposed to 5.5 mmol/L

Table 1. Primers for real-time PCR

Gene	Primer sequence
Beta-actin (rat)	Forward: CCCGCGAGTACAACCTTCTTG
	Reverse: GTCATCCATGGCGAACTGGTG
Runx2 (rat)	Forward: CCGAGACCAACCGAGTCATTTA
	Reverse: AAGAGGCTGTTTGACGCCAT
OCN (rat)	Forward: CTCAACAATGGACTTGGAGCC
	Reverse: GGCAACACATGCCCTAAACG
Osterix (rat)	Forward: GCCAGTAATCTTCGTGCCAG
	Reverse: TAGTGAGCTTCTTCCTGGGGA
TRAP (rat)	Forward: ATGACGCCAATGACAAGAGGTTCC
	Reverse: TTGTGCCGAGACATTGCCAAGG
CTSK (rat)	Forward: AGCAGTACAACAGCAAGGTGGATG
	Reverse: CACTTCTTCGCTGGTCATGTCTCC
GAPDH (mouse)	Forward: GGTTGTCTCCTGCGACTTCA
	Reverse: TGGTCCAGGGTTTCTTACTCC
TRAP (mouse)	Forward: GAACTTGCGACCATTGTTAGCC
	Reverse: CCGTTCTCGTCCTGAAGATACTG
RANK (mouse)	Forward: AGCCTCCGAGCAGAACTGACTC
	Reverse: CTGCCTGTGTAGCCATCTGTTGAG
TRAF-6 (mouse)	Forward: AGGAATCACTTGGCACGACACTTG
	Reverse: TGGTCCTGTCTTACTAGGCGACTC
CTSK (mouse)	Forward: GTGACCGTGATAATGTGAACCATG
	Reverse: CGTTGTTCTTATTCCGAGCCAAG

glucose (NG) medium and 44 mmol/L glucose (HG) medium. Cells were cultured for 2 days, after which the cells were administered BPs at concentrations of 10^{-6} mol/L, 10^{-7} mol/L, 10^{-8} mol/L, and 10^{-9} mol/L for 12 h, 24 h, 36 h, 48 h, and 72 h. Then, CCK-8 reagent (10 µl) was added to each well. After incubation at 37°C with 5% CO_2 for 3.5 h, the remaining solution was measured at 450 nm absorbance by a microplate reader (Thermo, USA).

Cytotoxic effects of BPs were measured by the WST-1 assay (Roche Diagnostics, Germany) according to the manufacturer's instructions. BMMs were seeded in 96-well plates ($1*10^3$ cells/well) under the same conditions as the osteoclastogenesis assays described above. In addition, RANKL-stimulated cells were exposed to NG medium and HG medium and incubated with various doses of BPs (10^{-6} mol/L, 10^{-7} mol/L, 10^{-8} mol/L, and 10^{-9} mol/L) for 48 h. Next, WST-1 (10 µl) reagent was added to each well. After incubation at 37°C with 5% CO_2 for 3 h, the remaining solution was measured with a microplate reader at 440 nm absorbance.

ALP staining and TRAP staining

BMSCs were cultured in six-well plates ($1*10^6$ cells/well) and cultivated in the presence of osteogenic inducers in three conditions (NG: 5.5 mmol/L glucose, HG: 44 mmol/L glucose, HG+BPs: 44 mmol/L glucose with 10^{-9} mol/L BPs) for 3 days. ALP activity was measured by using an ALP staining kit (Beyotime, China) in accordance with the manufacturer's instructions. Cells were fixed in 4% paraformaldehyde for 30 min at room temperature, washed three times with PBS and stained with ALP staining mixture for 30 min in the dark, after which the cells were rinsed three times with PBS to avoid nonspecific staining.

BMMs were seeded in 24-well plates ($1*10^4$ cells/well) with RANKL stimulation in the three conditions mentioned above for 6 days. Cellular TRAP staining was evaluated by using a phosphatase kit (Sigma-Aldrich, St. Louis). Briefly, cells were fixed and washed through the method mentioned above and incubated in a staining solution mixture in accordance with the manufacturer's instructions for 60 min in the dark, after which the cells were rinsed three times with PBS to avoid nonspecific staining. Then, mature osteoclasts, which manifested as positively stained cells with more than three nuclei, were counted under a light microscope (Leica DMI4000B, Germany) [27].

Quantitative real-time PCR (qRT-PCR)

qRT-PCR analysis was performed according to the previously described method [28]. Total RNA was extracted from osteogenic medium-cultured BMSCs and RANKL-stimulated mature osteoclasts at designated days using the TRIzol method according to the manufacturer's instructions. cDNA was extracted from 1 µg of total RNA using a Reverse Transcription System kit (Takara, Japan). PCR amplifications were performed using a DyNamo SYBR1 Green qPCR kit (Takara, Japan), and qRT-PCR was performed using a CFX Connect Real-Time PCR Detection System (Bio-Rad, USA). Relative gene expression levels were calculated and analyzed by the $2^{-\Delta\Delta CT}$ method with beta-actin or GAPDH as a control, and all reactions were analyzed in triplicate. The primer sequences (Sangon Biotech, Shanghai, China) are listed in **Table 1**.

Western blot analysis

Western blot analysis was conducted in accordance with a previously introduced method [29]. Cells were cultured in 60 mm petri dishes ($5*10^5$ cells/dish) for different periods according to the requirements. After washing three times with cold PBS, protein was extracted by RIPA lysis buffer (Santa Cruz Biotechnology, USA) with 1 mM phenylmethylsulfonyl fluoride (PMSF) (Beyotime, China). Total protein concentration was quantified by a bicinchoninic acid (BCA) protein assay kit (Beyotime, China). Equal amounts of protein extracts (40 μg) were loaded onto gels and analyzed by sodium dodecyl sulfate (SDS)-polyacrylamide gel electrophoresis (PAGE). Proteins were transferred to polyvinylidene difluoride membranes, after which the membranes were blocked with fat-free milk buffer and then incubated overnight at 4°C with primary antibodies against anti-Runx2 (1:2,000; Cell Signaling Technology), anti-β-actin (1:2,000; Cell Signaling Technology), anti-CTSK (1:1,000; Abcam), anti-RANK (1:1,000; Abcam) and anti-GAPDH (1:1,000; Abcam). The membranes were incubated with horseradish peroxidase-conjugated secondary antibodies (Abbkine, USA) at room temperature for 1 h. The Western blot bands were visualized by using an ECL Plus chemiluminescence reagent kit (Beyotime, China).

Biological characterization in vivo

Implant preparation: Commercially pure titanium implants (Fuxin Company, Baoji, China) with a length of 7 mm and a diameter of 1 mm were specifically designed in this study. After blasting with alumina particles and air pressure and washing with water, the implants were etched in a mixture of hydrochlorhydric acid (HA; Termira AuxiGel™, Sweden) (37 wt.%) and sulfuric acid (95 wt.%) at 80°C for 5 min, after which the implants were rinsed with demineralized water and air-dried. Then, the outermost porous structures of the implants were coated with a layer of HA (10-15 ml).

Crosslinked hyaluronic acid (Termira AuxiGel™, Sweden) was used as the drug delivery system for the BPs in this study [30-32]. The gels with BPs investigated by alendronate (4-amino-1-hydroxy-butylidene-1,1-bisphos-phonate; Hangzhou MSD Pharmaceutical Co. Ltd, China) was prepared as follows. First, BPs were dissolved with distilled water. Then, the crosslinked hyaluronic acid of the gel was synthesized. Finally, the BP solution was mixed with the crosslinked hydrogel. For the BPs group, administration at doses of 30 μg/kg was allowed to settle into the prepared hole before implants were inserted.

Animal model and study design

All animal experiments were conducted according to the U.K. Animals guidelines, the ARRIVE guidelines and the Guidelines for the Bioethics Committee for Animal Research of Chongqing Medical University. A total of 60 eight-week-old male SD rats were acquired from the Laboratory Animal Center of Chongqing Medical University (Chongqing, China) and housed under stabilized conditions at a temperature of 20°C, a humidity of 48% and on a 12-h light/dark cycle.

After 10 days of acclimatization, the rats were randomly divided into 3 groups, namely, the T2DM with BPs group (DM+BPs group, n=20), the T2DM without BPs group (DM group, n=20) and the sham-operated with vehicle group (N group, n=20). The rats in the N group were fed a standard diet, while T2DM was induced in the rats of the other two groups as previously described [33]. Briefly, fat accumulation and insulin resistance in T2DM rats were induced by a high-fat diet (40% fat, 42% carbohydrate, and 18% protein) for 4 weeks, and then, hyperglycemia was induced by intraperitoneal injection with streptozotocin (Sigma, USA) (30 mg/kg). Random blood glucose was measured with a glucometer (Roche, China) from the tail vein 72 h after injection. Twenty rats were selected for the next experiment with the criteria of random blood glucose ≥16.7 mmol/L. Four weeks after induction of diabetes, implants were inserted into the femoral condyles of rats under general anesthesia by 10% chloralhydrate. A cylindrical hole with a length of 10 mm and a diameter of 1.2 mm was created parallel to the long axis of the femora by a dental drill (SS WHITE BURS, America) with low rotational speed and external cooling with saline. Thereafter, implants of 30 μg/kg BP gel injections were applied to the holes. It was carefully ensured that the implants were placed in the same location of the femur on each side. No infections or other complications were found after the operation. The femora of 10 rats from

each group (n=20 per group: N, DM, DM+BPs) were harvested at 4 weeks, and the femora of the remaining rats were harvested at 8 weeks.

Double fluorescence labeling test

Tetracycline (30 mg/kg body weight; Sigma-Aldrich, USA) was administered intraperitoneally to animals for 19 days before sacrifice, while calcein (5 mg/kg body weight; Sigma-Aldrich, USA) was administered for 7 days. The specimens of the femora with implants (n=10 per group) were harvested at 4 or 8 weeks after implantation. The specimens were then fabricated into 30-µm slices and detected by confocal laser scanning microscopy (Leica, TCS. SP8, Germany). The regions that were 1000 µm away from the implant surface were measured by ImageJ software (Media Cybernetics, USA). The mineral apposition rate (MAR) was calculated, which indicated the ability of new bone to form.

Micro-CT analysis

Micro-CT (Vival CT 40, Scanco Medical, Switzer) was used to assess osteogenesis. Analysis of computerized images based on gray-level discrimination was performed. The regions of femora with implants ranging from 700 to 1000 were represented by gray values from 215 to 700. After scanning, 3D structures were reconstructed, and the defined region of interest (ROI) was identified as the total trabecular region around the implant with a radius of 500 µm from the first slice to the growth plate and including the distal 100 slices. The volumetric parameters were analyzed in accordance with guidelines from the American Society of Bone and Mineral Research (ASBMR) [34]. Briefly, the bone volume percentage (BV/TV), trabecular separation (Tb.S), trabecular thickness (Tb.Th) and trabecular number (Tb.N) were calculated.

Biomechanical test

Biomechanical tests were performed using a commercially available material testing system (Instron 4302; USA). To ensure equal stress loading on the femora specimens, the samples were immobilized in plastic molds. At the start of the test, a preload of 2 N defined the position of contact. Next, a vertical force parallel to the implant's longitudinal axis was applied with a displacement speed of 1 mm/min. Afterwards, the maximal push-out force and the ultimate shear strength were input into an excel spreadsheet, and load-deformation curves were plotted.

Histology and histomorphometry

After being dehydrated by 75% ethanol, the specimens were infiltrated in methyl methacrylate and then embedded in polymethylmethacrylate resin. After polishing, the specimens were stained with 1% toluidine. An optical microscope (Nikon Ti-S Eclipse, Japan) with a computer-coupled digital camera (ChemiDOC-TMXRS+imaging system; Bio-Rad, America) was used to observe the specimens and capture images. The regions 1000 µm from the surface of the implants were analyzed by ImageJ software. Bone tissue was colored purple, while soft tissue appeared blue in the stained regions. The bone-to-implant contact (BIC) was measured as the length percentage of the interface of bone and implant to the surface of the total implant, and the bone area ratio (BA) was calculated in a circular peri-implant ROI. All analyses were repeated at least three times.

Histology and immunohistochemistry examinations

TRAP staining was carried out using a kit (Sigma-Aldrich, St. Louis, USA) in accordance with the manufacturer's protocol. After incubation and staining according to the protocol, the specimens were observed by using an optical microscope (Nikon Ti-S Eclipse, Japan). Red-violet color was shown in the cytoplasm of osteoclasts by TRAP staining.

After fixing with 5% paraformaldehyde, the specimens were embedded in paraffin. Then, the 5 mm sections were incubated with osteocalcin (OCN) antibody (1:2,000; Cell Signaling Technology) according to the manufacturer's instructions. Brown-yellow cells exhibited osteogenic capability in the nuclei. The slides were further analyzed by optical microscopy (Nikon Ti-S Eclipse, Japan).

Expression analysis of relevant genes in vivo

Total RNA was extracted from the femora of mice in the three groups using the TRIzol method according to the manufacturer's protocols. Then, cDNA extraction and PCR amplification

were performed as described previously. Relative gene expression levels were calculated and analyzed by the $2^{-\Delta\Delta CT}$ method.

Statistical analysis

All statistical analyses were performed using the statistics package SPSS 17.0 (SPSS, USA). All data are presented as the mean ± standard deviation (SD). A *p*-value less than 0.05 according to one-way analysis of variance (ANOVA) indicated significant differences between groups. Pearson's correlation coefficients were calculated to assess the relationships among micro-CT, histological, and biomechanical parameters.

Results

Effects of BPs on the osteogenic differentiation of BMSCs in the high glucose condition

Calcium nodule deposition and lipid droplets demonstrated the capability of osteogenesis and adipogenesis (**Figure 1Aa-Ac**). To filter the optimal concentration and detect cell proliferation, BMSCs were treated with BPs at various concentrations for different periods of time. The BPs group showed a significant increase in BMSC proliferation, particularly at lower concentrations of BPs (10^{-9} mmol/L) (P<0.05, **Figure 1B**). Therefore, lower concentrations of BPs (10^{-9} mmol/L) were applied to the in vitro study. To investigate the effects of HG or BPs on the mineralization process of BMSCs, cells were cultivated in mineralizing medium, and then, ALP staining was performed. A significant reduction in mineralization was demonstrated in the HG group by ALP staining; in contrast, the BPs group displayed the opposite result (**Figure 1D**). Additionally, HG markedly reduced the expression of Runx2, OCN and Osterix in BMSCs; however, gene expression in the BPs group was higher than that in the HG group (**Figure 1E**) as shown by qRT-PCR. A remarkable increase in the protein level of Runx2 was observed in the BPs group compared with the HG group, and this increase occurred simultaneously with the upregulation of β-catenin (**Figure 1F** and **1G**).

Effects of BPs on osteoclast differentiation in high glucose conditions

BMMs in the BPs groups were treated with RANKL and BPs at a concentration of 10^{-9} mmol/L for 7 days. Multinucleated cells,

defined as those with 3 or more nuclei, were identified as osteoclasts and counted by TRAP staining (**Figure 1Ad**). Moreover, we investigated whether BPs at the indicated doses had cytotoxic effects on osteoclast differentiation (**Figure 1C**). Significantly more multinucleated osteoclasts had formed in the HG group. Interestingly, treatment with BPs was discovered to decrease the amounts of TRAP-positive cells and inhibit the differentiation of osteoclasts (**Figure 2A** and **2B**). These results indicated that relatively lower concentrations of BPs (10^{-9} mmol/L) inhibited the differentiation of osteoclasts without cytotoxicity. The mRNA expression levels of TRAP, RANK, TRAF-6, and CTSK were enhanced in the HG condition but were decreased in the BPs group compared with the HG group (**Figure 2C**). Additionally, the protein expression of RANK and CTSK was remarkably reduced by BPs treatment compared with HG without BPs (**Figure 2D** and **2E**). These results suggest that lower concentrations of BPs suppress the formation of osteoclasts through the expression of osteoclast-specific genes and proteins.

Establishment of the T2DM rat model and implant surgery

Consistent with a previous study, diabetic rats showed histopathological changes such as pancreatic islets, β-cells and trabecular microarchitectures [35]. The area of pancreatic islets was markedly reduced, and β-cells appeared to exhibit marked injury in T2DM rats (**Figure 3B**). Meanwhile, decreased bone mass and impaired trabecular microarchitectures were revealed by X-ray, histological images and micro-CT in T2DM rats (**Figure 3C**, **3D** and **3F**).

All T2DM rats survived after anesthesia without diabetic complications except one. Four weeks after inducing fat accumulation and insulin resistance, glucose levels were examined (**Figure 3G**). More remarkable changes in glucose levels were found in the DM group than in the N group (P<0.05). After STZ injection, there were no significant differences in body weight (P>0.05) or insulin levels (P>0.05) between the DM and N groups.

After blasting, etching, rinsing and air drying, the implants were coated with a layer of HA. The surface morphology of the implants was evaluated by scanning electron microscopy (SEM) with or without grit-blasting and etching (**Figure 4A**). 3D structures were reconstructed,
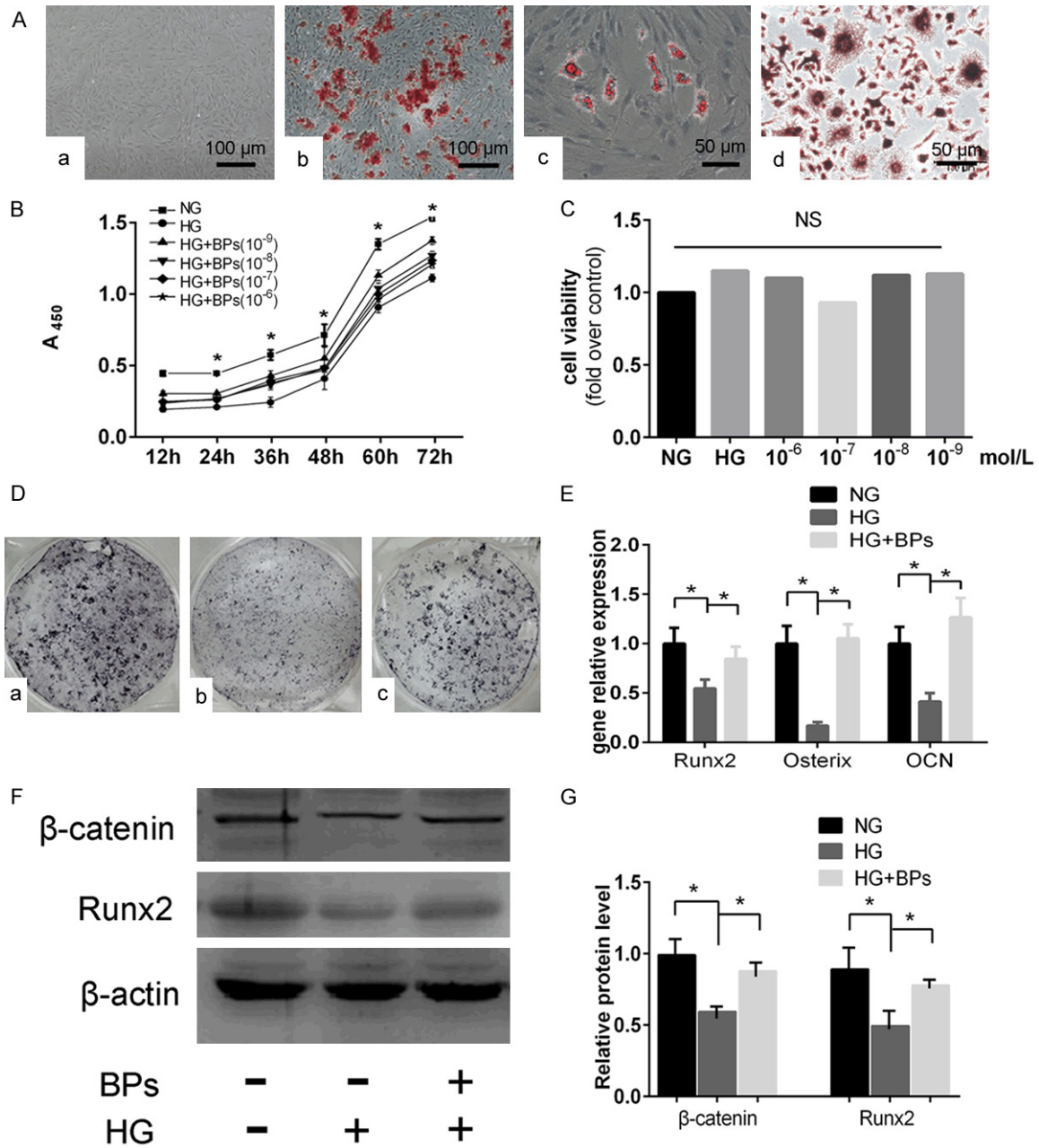
Figure 1. Cell identification, concentration filtering and osteogenic differentiation of BMSCs in vitro. A, a. An image of cultured BMSCs grown in DMEM (original magnification *200). b. BMSCs differentiated into osteoblasts and stained with Alizarin red (original magnification *200). c. BMSCs differentiated into adipocytes and stained with Oil Red O (original magnification *400). d. BMMS differentiated into osteoclasts and stained with TRAP (original magnification *400). B. Assessment of cell proliferation and filtering of optimal concentration by CCK-8, NG: 5.5 mmol/L glucose, HG: 44 mmol/L glucose, HG+BPs: 44 mmol/L glucose with BPs of 10^{-6} mol/L, 10^{-7} mol/L, 10^{-8} mol/L, and 10^{-9} mol/L for 12 h, 24 h, 36 h, 48 h, and 72 h). Experiments were performed at least in triplicate, and the data are expressed as the mean ± SD (n=6). C. Assessment of cell viability of high glucose or BPs on osteoclast formation (NG: 5.5 mmol/L glucose, HG: 44 mmol/L glucose, HG+BPs: 44 mmol/L glucose with BPs of 10^{-6} mol/L, 10^{-7} mol/L, 10^{-8} mol/L, and 10^{-9} mol/L for 48 h culturing). Experiments were performed at least in triplicate, and the data are expressed as the mean ± SD (n=6). D. ALP staining for osteoblastogenesis of BMSCs affected by BPs. a. NG group: 5.5 mmol/L glucose. b. HG group 44 mmol/L glucose. c. HG+BPs: 44 mmol/L glucose + 10^{-9} mol/L BPs. E. Runx2, OCN and Osterix expression during osteogenesis. Experiments were performed at least in triplicate, and the data are expressed as the mean ± SD (n=3). *P<0.05. (by ANOVA); F, G. Runx2 and β-catenin protein were detected by Western blot. Experiments were performed at least in triplicate. These data are expressed as the mean ± SD (n=3). *P<0.05 (by ANOVA).
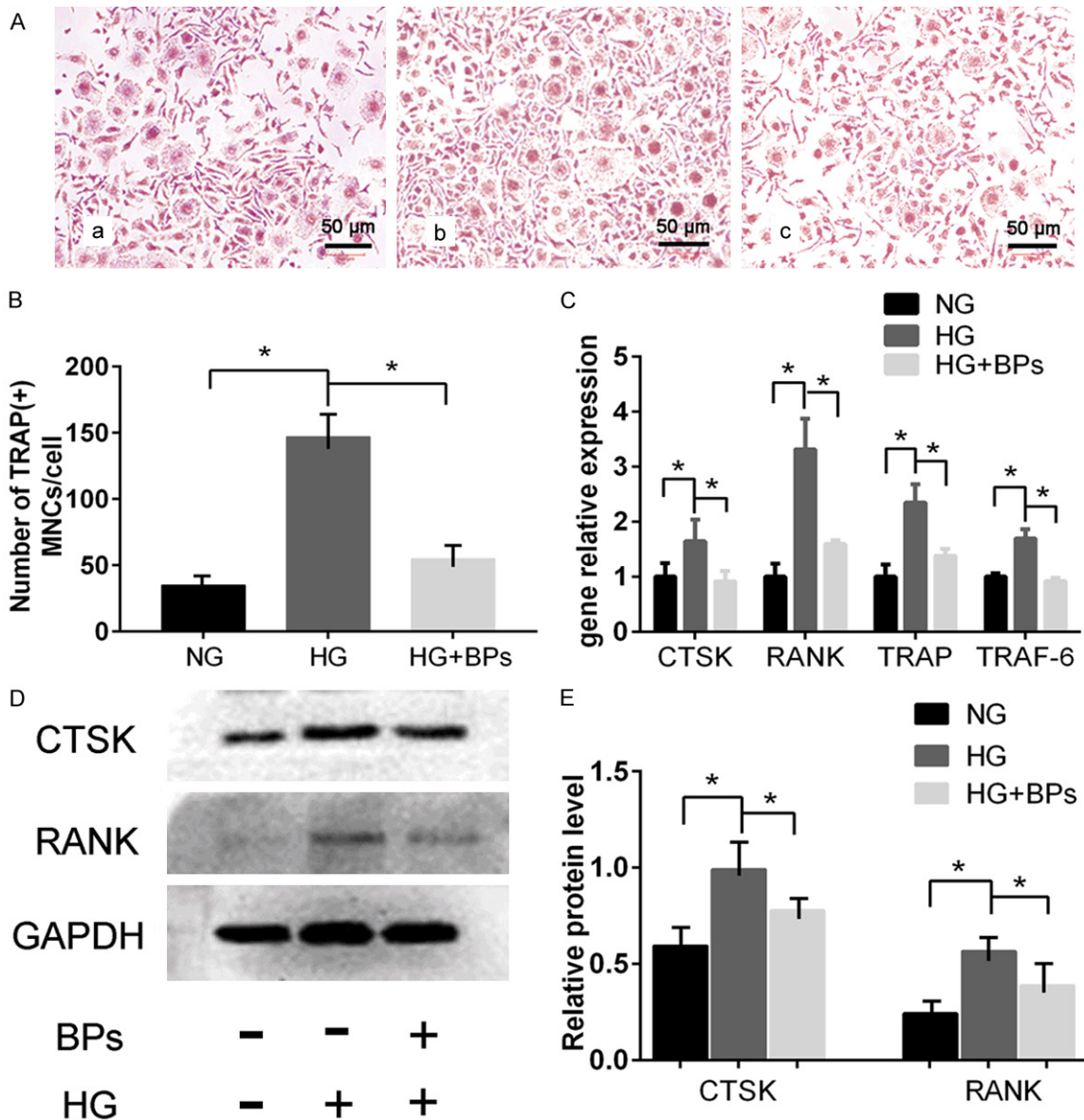
Figure 2. In vitro experiment of osteoclast differentiation of BMMs. BMMs in the BPs group were treated with RANKL and BPs at a concentration of 10^{-9} mmol/L for 7 days. A. TRAP staining for osteoclastogenesis of BMMs affected by BPs (original magnification *400). a. 5.5 mmol/L glucose. b. 44 mmol/L glucose. c. 44 mmol/L glucose + 10^{-9} mol/L BPs. B. Number of TRAP-positive multinucleated cells (MNCs) on day 6. Experiments were performed at least in triplicate, and the data are shown as the means ± SD (n=3). *P<0.05 (by ANOVA). C. TRAF-6, TRAP, RANK, and CTSK expression during osteoclastogenesis. Experiments were performed at least in triplicate. The data are expressed as the mean ± SD (n=3). *P<0.05 (by ANOVA). D, E. RANK and CTSK protein were detected by Western blot. The cells were induced by three different stimulators of osteoclastogenesis for 6 days. Experiments were performed at least in triplicate, and the data are expressed as the mean ± SD (n=3). *P<0.05 (by ANOVA).

and the ROI was identified as the total trabecular section around the implant with a radius of 500 μm from the first slice to the growth plate and then to the distal 100 slices (**Figure 4B**). Four weeks after induction of diabetes, the implants were inserted into holes created parallel to the long axis of the femora, as described above, under general anesthesia (**Figure 4C**). Local administration of the crosslinked hyaluronic acid of the gel was allowed to settle into the prepared holes in the BPs group before the implants were inserted. The BPs showed relatively rapid release in the first 7 h, followed by a steady release phase (**Figure 4D**).
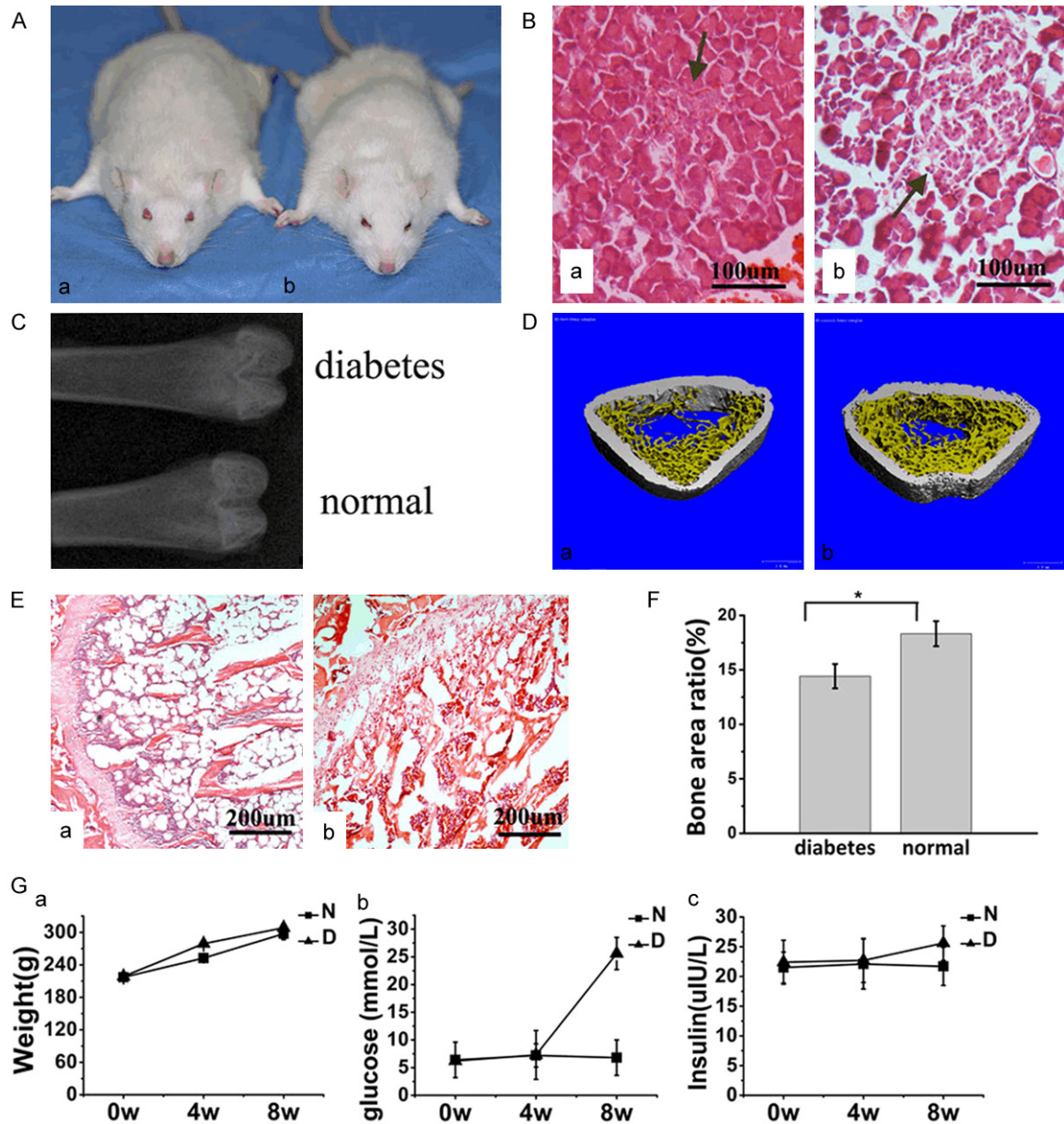
Figure 3. Establishment of type-2 diabetic rat model. A, a. Diabetic rat. b. Normal rat. General morphology of the rats. B, a. Diabetic rat. b. Normal rat. Histological staining of sections of the pancreas (HE staining, original magnification *200). The area of pancreatic islets was markedly reduced, and β-cells appeared to exhibit marked injury in T2DM rats. Decreased bone mass and impaired trabecular microarchitectures were evaluated by X-ray, histological images and micro-CT in T2DM rats. C. X-ray of the proximal femora through the longitudinal plane. D, a. Diabetic rat. b. Normal rat. Micro-CT of the distal femora through the transversal plane. E, a. Diabetic rat. b. Normal rat. Histological sections of the distal femora through the transverse plane (HE staining, original magnification *100). F. Statistical results of BA according to histomorphometry. Experiments were performed in at least triplicate. Data are expressed as the mean ± SD (n=2). *P<0.05 (by ANOVA). Experiments were performed at least in triplicate. G. The changes in body weight, glucose level, and insulin level between the two groups tended to reveal more remarkable changes in glucose levels in the DM group than in the N group. Among the rats after STZ injection, there were no significant differences in body weight or insulin levels between the DM and N groups. Experiments were performed at least in triplicate. The data are expressed as the mean ± SD (n=2). *P<0.05 (by ANOVA).

Comparing the osseointegration

The femoral specimens of 10 rats from each group (n=20 per group: N, DM, DM+BPs) were

harvested at 4 weeks, and the remaining specimens were harvested at 8 weeks (**Figure 5A**). The double fluorescence labeling method of calcein and tetracycline was adopted. The bone
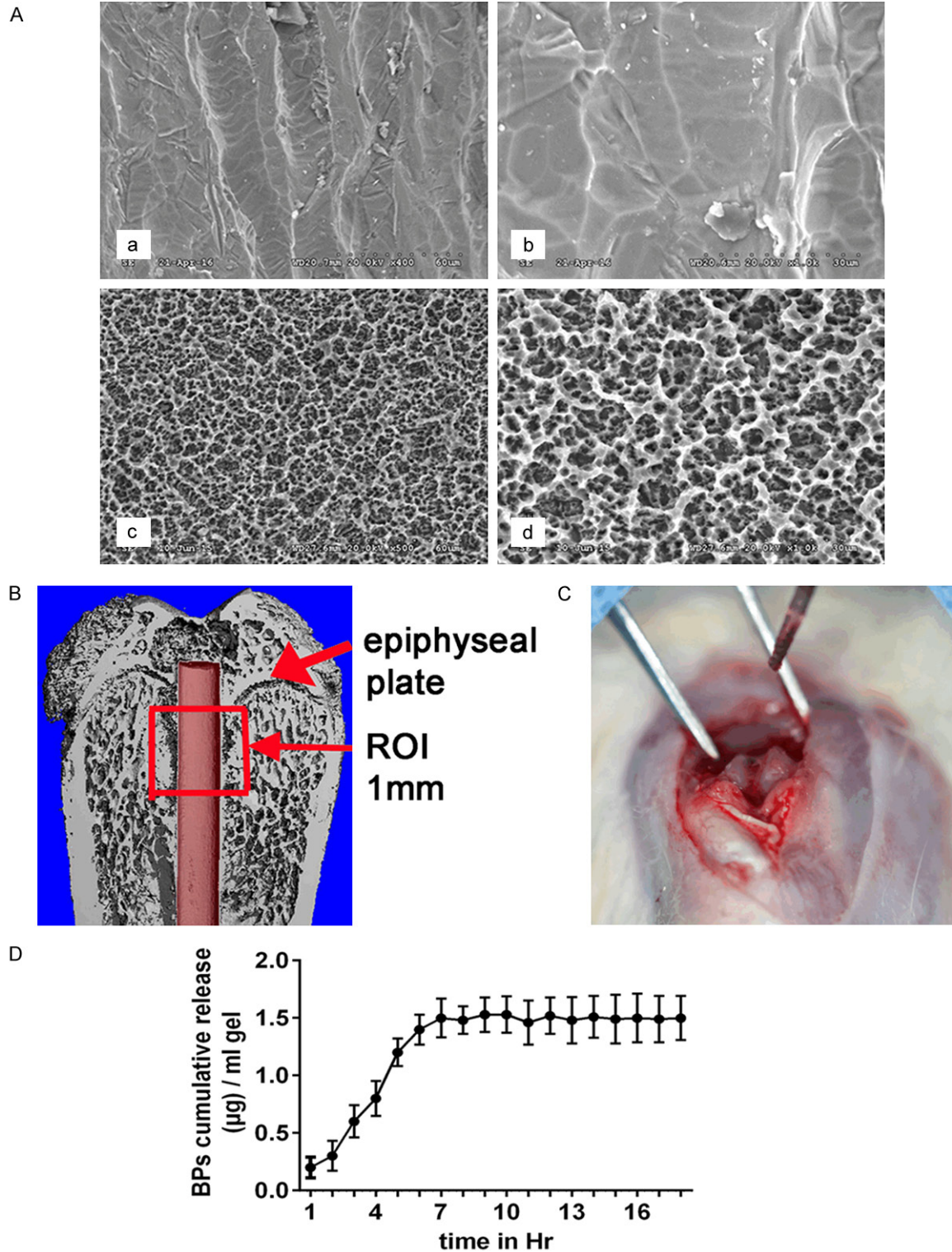
Figure 4. Implant surgery and the mode of BP release. A. Surface morphology of implants observed using a scanning electron microscope (SEM). a, b. Without grit-blasting and etching. c, d. With grit-blasting and etching). B. Schematic of the region of interest (ROI) in the micro-CT evaluation. The defined ROI was identified as the total trabecular section around the implant with a radius of 500 μm from the first slice to the growth plate and then to the distal 100 slices. C. Prepared implant hole. The implants were inserted into the holes created parallel to the long axis of the femora. D. The cumulative amount of BPs released from 1 mg of crosslinked hyaluronic acid in the gel. The BPs showed relatively rapid release in the first 7 h, continued by a steady release phase.
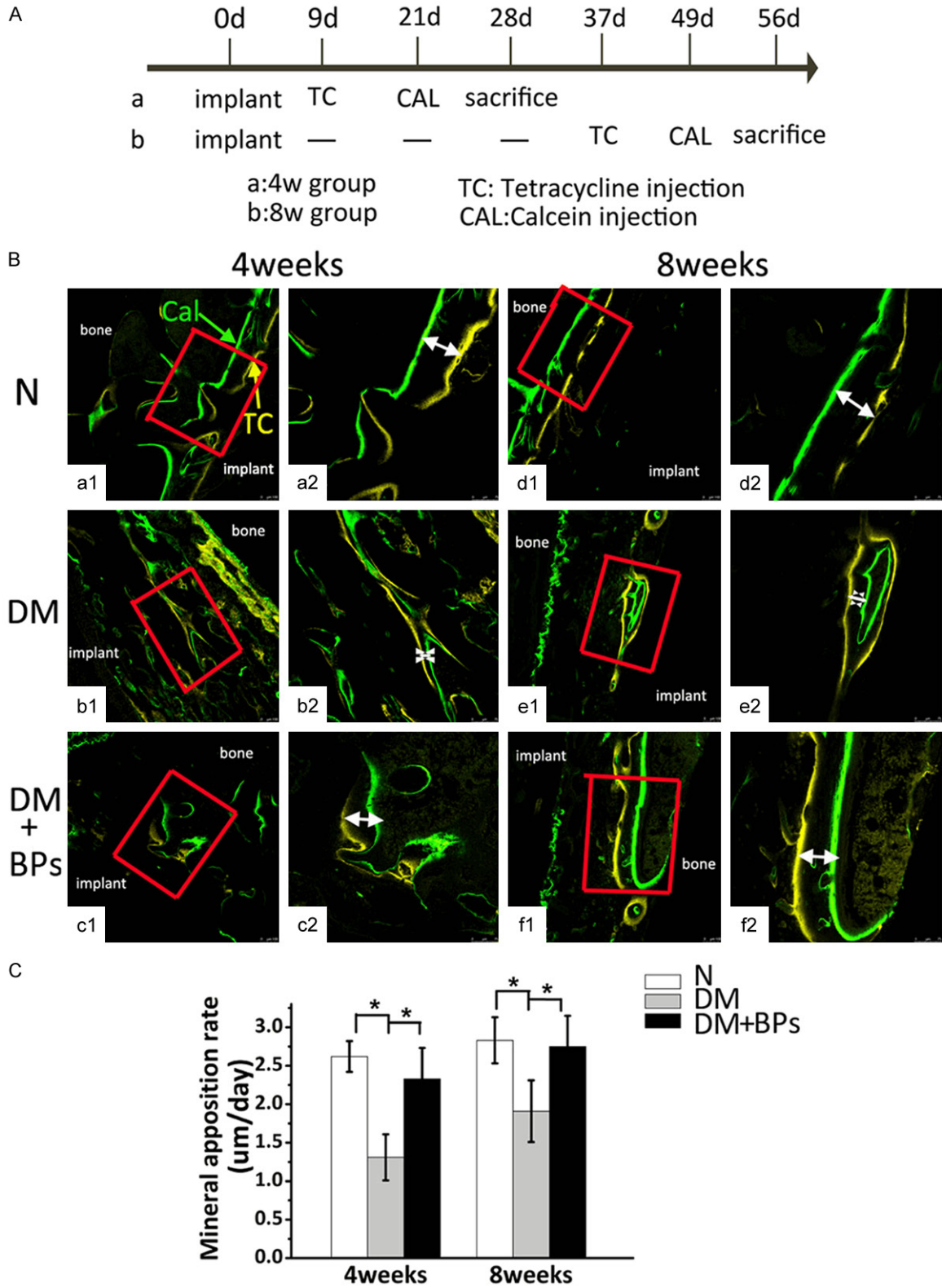
Figure 5. Results of the double fluorescence labeling analysis. (A) Timeline for the experiment. The femoral specimens of 10 rats from each group (n=20 per group: N, DM, DM+BPs) were harvested at 4 weeks, and the remaining specimens were harvested at 8 weeks. (B) Double fluorescence labeling image scanning was performed by confocal laser scanning microscopy (a1-f1, magnification *100; a2-f2, magnification *200). Double labeling lines, including

yellow (representing tetracycline staining) and green (representing calcein staining), could be observed in the peri-implant bone in each group by confocal laser scanning. The white arrows indicate the distance between the two lines. (C) MAR values after 4 weeks and 8 weeks in the N, DM, and DM+BPs groups. Experiments were performed at least in triplicate. The data are expressed as the mean ± SD (n=3). *P<0.05 (by ANOVA).

mineral deposition rate was analyzed to investigate the bone formation activity. Double labeling lines, including yellow (representing tetracycline staining) and green (representing calcein staining), could be observed in peri-implant bone in each group by confocal laser scanning (**Figure 5B**). Four weeks after implantation, the formation of active new bone was found in each group by fluorescence labeling. Data revealed that the MAR of the N group (2.62 μm/day) was the highest, followed by the DM+BPs group (2.33 μm/day), and the MAR of DM group (1.31 μm/day) was the lowest. Eight weeks after implantation, similar findings were observed among the three groups by confocal laser scanning, with MAR values of 2.83 μm/day, 1.91 μm/day, and 2.75 μm/day in the N group, DM group, and DM+BPs group, respectively (**Figure 5B** and **5C**). The results revealed that local administration of BPs played a role in promoting bone formation, which reversed the reduced MAR levels of the DM group.

The bone-implant interface and the trabecular microstructure of the peri-implant bone tissue among the N, DM, and DM+BPs groups were analyzed by micro-CT (**Figure 6A** and **6B**). The results of the micro-CT analysis are shown in **Table 2**. The DM+BPs group exhibited significantly higher BV/TV, Tb.Th, Tb.N and significantly lower Tb.Sp than the DM group after both 4 and 8 weeks of implantation. Compared with the T2DM group, BV/TV, Tb.N, and Tb.Th increased by 140% (P<0.05), 62% (P<0.05), and 40% (P<0.05), respectively, and Tb.Sp decreased by 48% (P<0.05) by 4 weeks after implantation, respectively, in the DM+BPs group. Additionally, at 8 weeks after implantation, BV/TV, Tb.N, and Tb.Th increased by 121% (P<0.05), 49% (P<0.05), and 40% (P<0.05), respectively, and Tb.Sp decreased by 54% (P<0.05) (**Figure 6C**).

For histological and histomorphometric analysis, the specimens were stained with 1% toluidine. Bone tissue was colored purple, while soft tissue appeared blue in the stained regions (**Figure 7A**). BIC was measured as the percentage of the area of the bone-implant interface to the surface area of the total implant, and BA was calculated in a circular peri-implant ROI.

The undecalcified sections according to bone histomorphometry revealed that BPs had a significant effect on osseointegration in the DM group (P<0.05, **Figure 7B**). Additionally, the significant correlation coefficients between the histological and biomechanical parameters were shown by intergroup comparison (P<0.05, **Table 3**). Correspondingly, quantification analysis revealed that fixation of implantation was significantly related to histological factors.

The biomechanical parameters, namely, the maximal push-out force and the ultimate shear strength, as shown in **Table 2**, demonstrated that there were significant increases in the maximal push-out force (P<0.05) and the ultimate shear strength (P<0.05) in the DM+BPs group compared with the DM group (**Figure 7C**). The micro-CT and biomechanical parameters analyzed by intergroup comparison showed significant correlation (P<0.05, **Table 3**), which indicated a strong relationship between the strength of the bone-implant osseointegration and the microarchitecture.

Significantly more multinucleated osteoclasts were found in the DM group by TRAP staining. Similar to the results of the in vitro study, the addition of BPs was discovered to decrease the amount of TRAP-positive cells and inhibit the differentiation of osteoclasts (**Figure 8A** and **8B**). Additionally, the results of immunohistochemical staining for OCN demonstrated that there were significant increases in the osteogenic capability in the DM+BPs group compared with the DM group (**Figure 8D**).

The mRNA expression levels of Runx2 and OCN extracted from the femora of mice in the DM group were lower than those in the N group; however, gene expression after the addition of BPs increased. Similar to the results of the in vitro study, the mRNA expression levels of TRAP and CTSK extracted from the femora of mice were enhanced in the DM group but decreased by BP exposure (**Figure 8C**).

Discussion

Patients with T2DM are at higher risk of suffering a fracture, particularly fracture of the lower
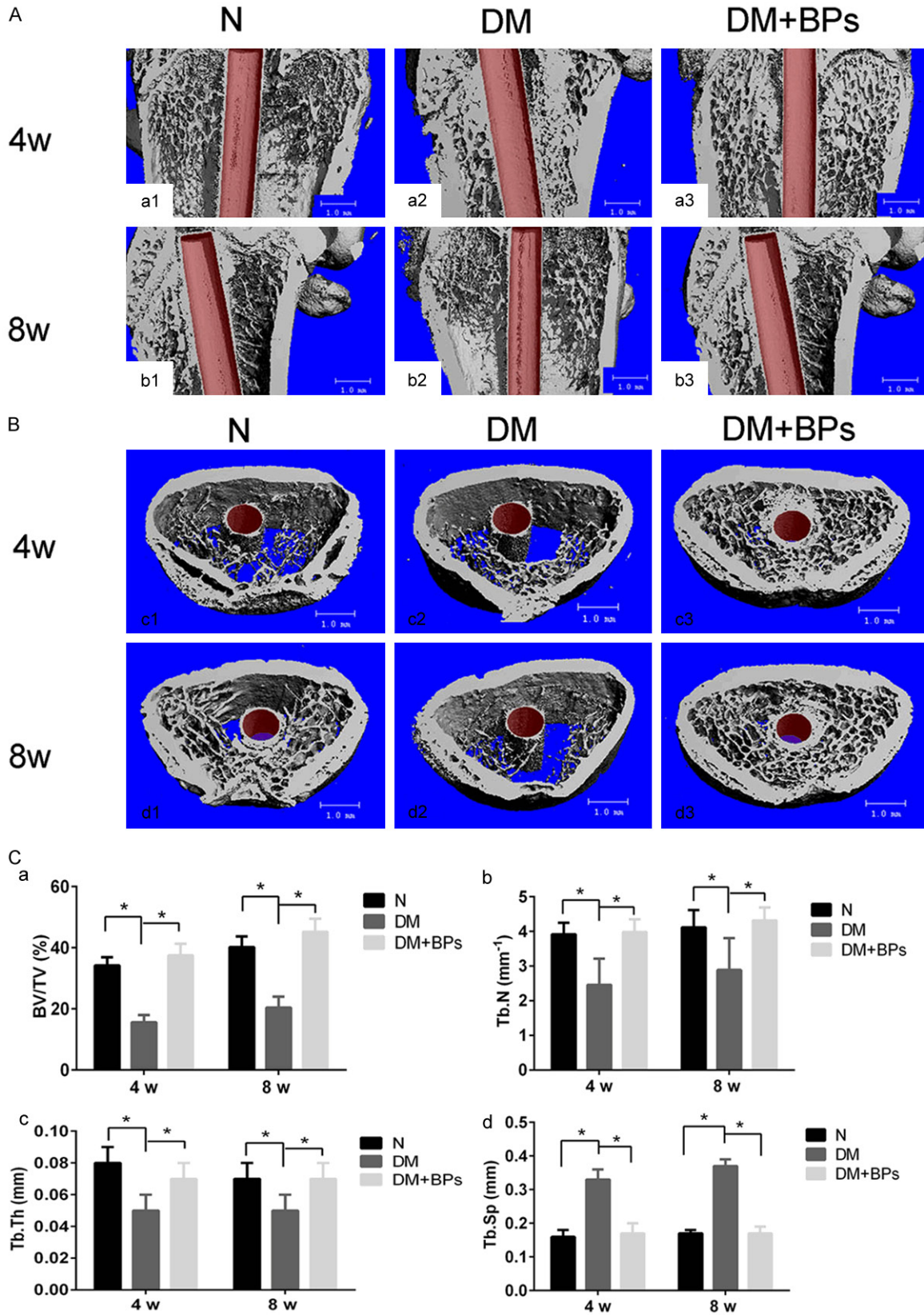
A

B

C

Figure 6. Micro-CT images of femora with implants. A, B. Micro-CT images of the ROI. The bone-implant interface and the trabecular microstructure of the peri-implant bone tissue among the three groups were analyzed by micro-CT.

C. Statistical results of BV/TV, Tb.Th, Tb.N and Tb.Sp according to micro-CT at 4 weeks and 8 weeks after implant insertion in the N, DM and DM+BPs groups, respectively. Experiments were performed at least in triplicate. The data are expressed as the mean ± SD (n=3). *P<0.05 (by ANOVA).

Table 2. Quantitative results of implant osseointegration, peri-implant trabeculae by micro-CT assessment and biomechanical testing at 4 weeks and 8 weeks after implant insertion in the N, DM and DM+BPs groups

	N		DM		DM+BPs	
	4 weeks	8 weeks	4 weeks	8 weeks	4 weeks	8 weeks
BV/TV (%)	34.21 ± 2.66	40.24 ± 3.44	15.65 ± 2.31[a]	20.43 ± 3.62[b]	37.52 ± 3.74[c]	45.22 ± 4.23[d]
Tb.N (mm^{-1})	3.92 ± 0.33	4.12 ± 0.45	2.46 ± 0.76[a]	2.89 ± 0.92[b]	3.98 ± 0.37[c]	4.32 ± 0.37[d]
Tb.Th (mm)	0.08 ± 0.01	0.07 ± 0.01	0.05 ± 0.01[a]	0.05 ± 0.01[b]	0.07 ± 0.01[c]	0.07 ± 0.01[d]
Tb.Sp (mm)	0.16 ± 0.02	0.17 ± 0.01	0.33 ± 0.03[a]	0.37 ± 0.02[b]	0.17 ± 0.03[c]	0.17 ± 0.02[d]
Maximal push-out force (N)	83.2 ± 3.5	145.4 ± 5.8	39.7 ± 4.1[a]	61.6 ± 3.7[b]	65.1 ± 5.5[c]	101.2 ± 6.2[d]
Ultimate shear strength (N/mm^2)	5.8 ± 1.2	9.4 ± 2.1	2.3 ± 1.9[a]	3.6 ± 0.6[b]	4.8 ± 1.1[c]	6.9 ± 1.8[d]

Note: N: healthy rats; DM: T2DM rats without BPs administration; DM+BPs: T2DM rats treated with BPs; BV/TV: percentage of bone volume; Tb.S: trabecular separation; Tb.Th: trabecular thickness; Tb.N: trabecular number; Data are expressed as the mean ± SD (n=20); a, vs. the N group at 4 weeks, P<0.05; b, vs. the N group at 8 weeks, P<0.05; c, vs. The DM group at 4 weeks, P<0.05; d, vs. The DM group at 8 weeks, P<0.05 (by ANOVA).

extremities and hip [36], while other reports have revealed an increased risk of vertebral fracture [37]. A recent survey conducted by the International Diabetes Federation (IDF) asserted that there were almost 425 million individuals suffering from T2DM in 2017 worldwide and predicted that this number could possibly exceed 645 million by 2045 [38]. Streptozotocin-induced T2DM in rats is a well-characterized animal model for diabetes investigation [39]. Emerging evidence indicates that the impairment of bone metabolism in osteoporosis is closely related to the pathogenesis of glucose intolerance, insulin resistance and T2DM [40]. We investigated the injection of streptozotocin in rats, resulting in the breaking of pancreatic β-cells, remarkable hyperglycemia and weight loss, while simultaneously leading to lower bone density, decreased biomechanical quality, and destruction of the microarchitecture of the femora in rats, in agreement with the report of Srinivasan K et al [33].

Due to the limited size and form of the jaw in rats, femora have been widely used for studies that have suggested reduced implant-bone repair in DM-induced animal models (rats) [41]. Studies using rats as an osteoporotic model have reported decreased bone mass, reduced bone turnover, and reduced implant-bone contact area [42]. Thus, we established diabetic osteoporosis with a rat model and then inserted implants into the proximal femora. Compared with sham rats, there were remarkable changes in rats in the DM group. The results of this

study suggest that treatment can fail in individuals suffering from type 2 diabetic osteoporosis due to decreased bone mass around implants or unsuccessful osseointegration, eventually resulting in implant failure.

BPs integrated with calcium crystals serve as the first-line treatment for osteoporosis. A systematic review reported that administration of systemic BPs facilitated implant osseointegration in a rat model with induced osteoporosis [43]. In consideration of the complications related to systemically administered BPs, [15], studies investigating how to avoid side effects are needed. Complications can be averted by local administration of BPs, which has been concluded in the literature [44]. Mathijssen NM et al [45] reported that local administration of BPs likely played a critical role in increasing the success rate of surgery, such as bone defect restoration and promoting stability. Furthermore, Miettinen et al [46] reported that local injections of BPs may be effective for accelerating bone regeneration and that the positive effects on new bone formation can be explained by its activity on bone. Cuairán C [47] results showed that locally delivered zoledronate at a low dose improved the stability of miniscrew implants over time. Thus far, there is no clear indication of the minimal dose of BPs that can protect bone structure and mitigate bone resorption in patients suffering from osteoporosis [48]. Accordingly, we reported that the treatment of BPs with local application after T2DM pathogenesis of may inhibit bone
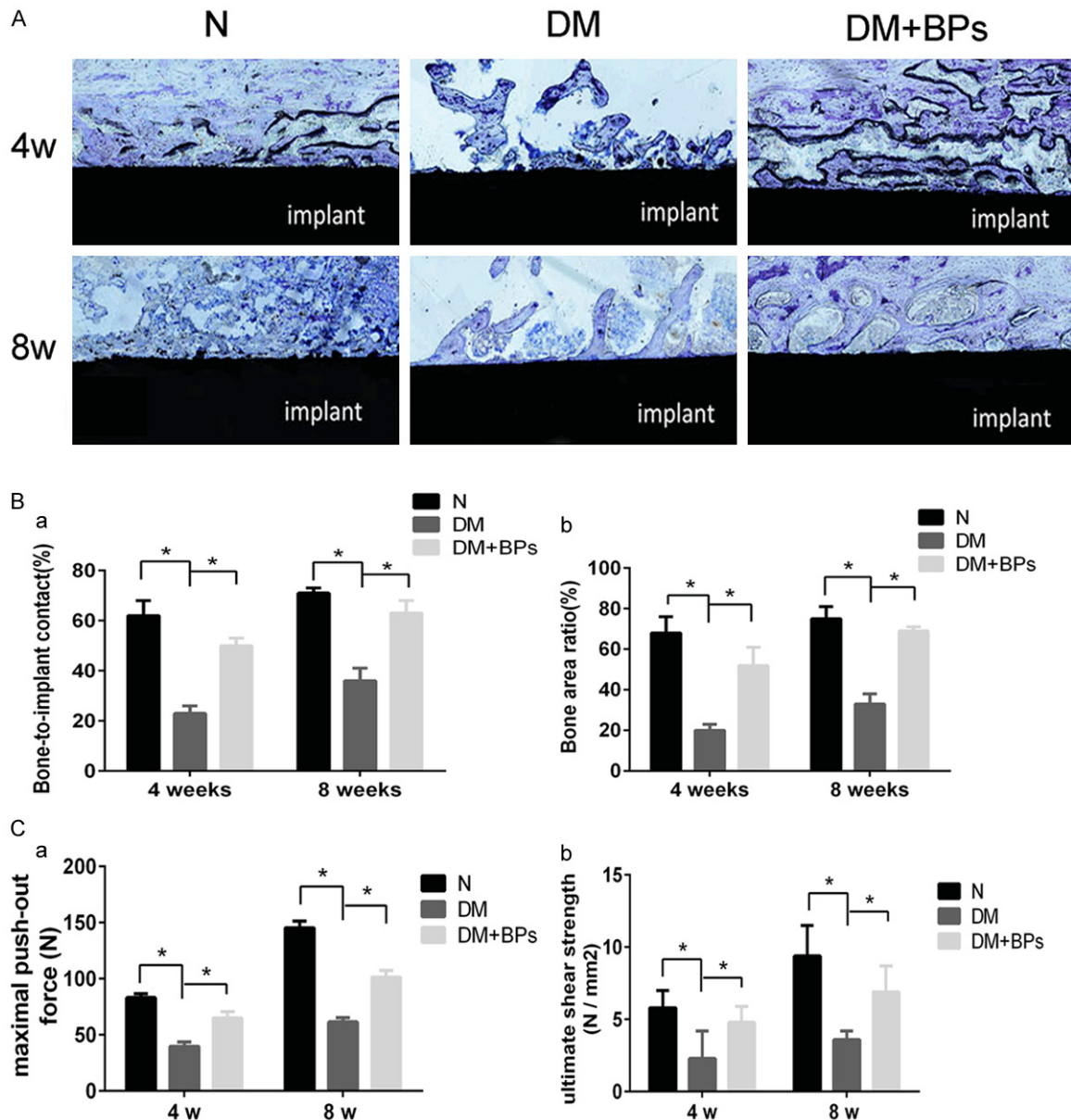
Figure 7. Results of histological evaluation and biomechanical test analysis. (A) Toluidine staining. All histological sections are located approximately 1 mm below the epiphyseal plate of the femora. (B, a, b) Statistical results of BIC (a) and BA (b) according to histomorphometry. Experiments were performed at least in triplicate, and the data are expressed as the mean ± SD (n=3). *P<0.05 (by ANOVA). (C, a, b) Statistical results of the maximal push-out force and the ultimate shear strength according to biomechanical testing at 4 weeks and 8 weeks after implant insertion. Experiments were performed at least in triplicate, and the data are expressed as the mean ± SD (n=3). *P<0.05 (by ANOVA).

loss and promote bone quality, which can reverse eventual implant failure.

In this respect, fixation of the BPs onto the surface of the implant has been tested as one method for delivering the drug locally and efficiently [49]. In a report by Guimaraes et al [19], direct application of BPs gel was injected into the surgical cavity before implant insertion, whereas Jakobsen et al [50] reported soaking materials in BPs solution prior to insertion into the surgical cavity. However, existing studies have illustrated a lack of standardization in the method of local delivery of BPs to surgical areas. The BP gel formulated in this study was prepared following the protocol reported by

Table 3. Intergroup correlation analysis among micro-CT, histological and biomechanical test parameters

Pearson correlation	Micro-CT and histological parameters	Maximal push-out force (N)	Ultimate shear strength (N/mm^2)
4 weeks	BV/TV	0.735*	0.683*
	Tb.N	0.634*	0.624*
	Tb.Th	0.643*	0.659*
	Tb.Sp	-0.632*	-0.682*
	BA	0.725*	0.784*
	BIC	0.754*	0.643*
8 weeks	BV/TV	0.781*	0.742*
	Tb.N	0.662*	0.632*
	Tb.Th	0.658*	0.776*
	Tb.Sp	-0.667*	-0.672*
	BA	0.731*	0.692*
	BIC	0.771*	0.619*

Note: BV/TV: percentage of bone volume; Tb.S: trabecular separation; Tb.Th: trabecular thickness; Tb.N: trabecular number; BA: bone area ratio; BIC: bone-to-implant contact. The significant correlation coefficients among the parameters of micro-CT, histological and biomechanical tests are shown according to the intergroup comparisons. *P<0.05 (by Pearson's correlation coefficients).

Kettenberger U and Ston J [31], and this gel was used to release BPs into the surgical area before implant placement. By employing the method developed in this study, the local application of BP gel promoted osseointegration, supporting the initial hypothesis of the study.

In the in vivo study, implants were placed into the proximal femora of rats, and then, the rats were treated with BPs at a dose of 30 µg/kg, as previously described. The stability of implants can be represented by the level of osseointegration, which can be influenced by the quality and quantity of bone in the surgical area after implantation [51]. Although may rodent models of T2DM have been developed in the literature, few studies have evaluated bone metabolism and stress. The intergroup comparisons showed significant correlations among the micro-CT, histological and biomechanical parameters (P<0.05), which indicated a strong relationship between the bone-implant osseointegration strength and the microarchitecture. These findings strengthen the conclusions of this study.

The health of bone relies on a relative balance between two types of cells that are devoted to bone formation and bone reabsorption: osteoblasts and osteoclasts. The imbalanced activity of osteoclasts and osteoblasts in metabolic processes is common in a variety of bone diseases [52]. The mechanism of how BPs act on osteoblasts and osteoclasts remains unclear, despite many years of investigation, although some evidence has emerged [53]. Osteoclasts are derived from the fusion of mononuclear phagocytes, the precursors of osteoclasts differentiated under the effects of two cytokines, M-CSF and RANKL, which are located in peripheral blood [54]. RANKL, a membrane-combined protein, is located on osteoblasts and some stromal cells, which facilitates the differentiation and fusion of osteoclast precursors and mature osteoclasts by combining RANK [55]. The expression of RANK influences the recruitment of osteoclast-specific genes and markers such as TRAF6, TRAP and CTSK, which represent the differentiation and activation of osteoclasts [56]. Our in vitro study results demonstrated that HG stimulates bone resorption, while relatively low-dose BPs suppress the formation of osteoclasts through the expression of osteoclast-specific genes and proteins. During the bone resorption process, osteoclasts serve as the primary target for BPs, which can liberate and internalize minerals [57]. The influences of BPs on osteoblasts are being gradually discovered, which raises the question of whether BPs can interact with bone formation activity [58]. Lu H et al [59] concluded that the influences of a hyperglycemic condition have been indicated to inhibit the differentiation of osteoblasts and the formation of collagen, leading to decreased bone formation and weakened quality of the newly formed bone. Because bone-forming activity is closely associated with bone-reabsorbing activity, it is possible to speculate that bone remodeling could be inhibited by the presence of a hyperglycemic state. However, controversy exists as to whether the function of osteoblasts and the mineralization process might be inhibited by BPs [60]. Osteoblasts are derived from multipo-
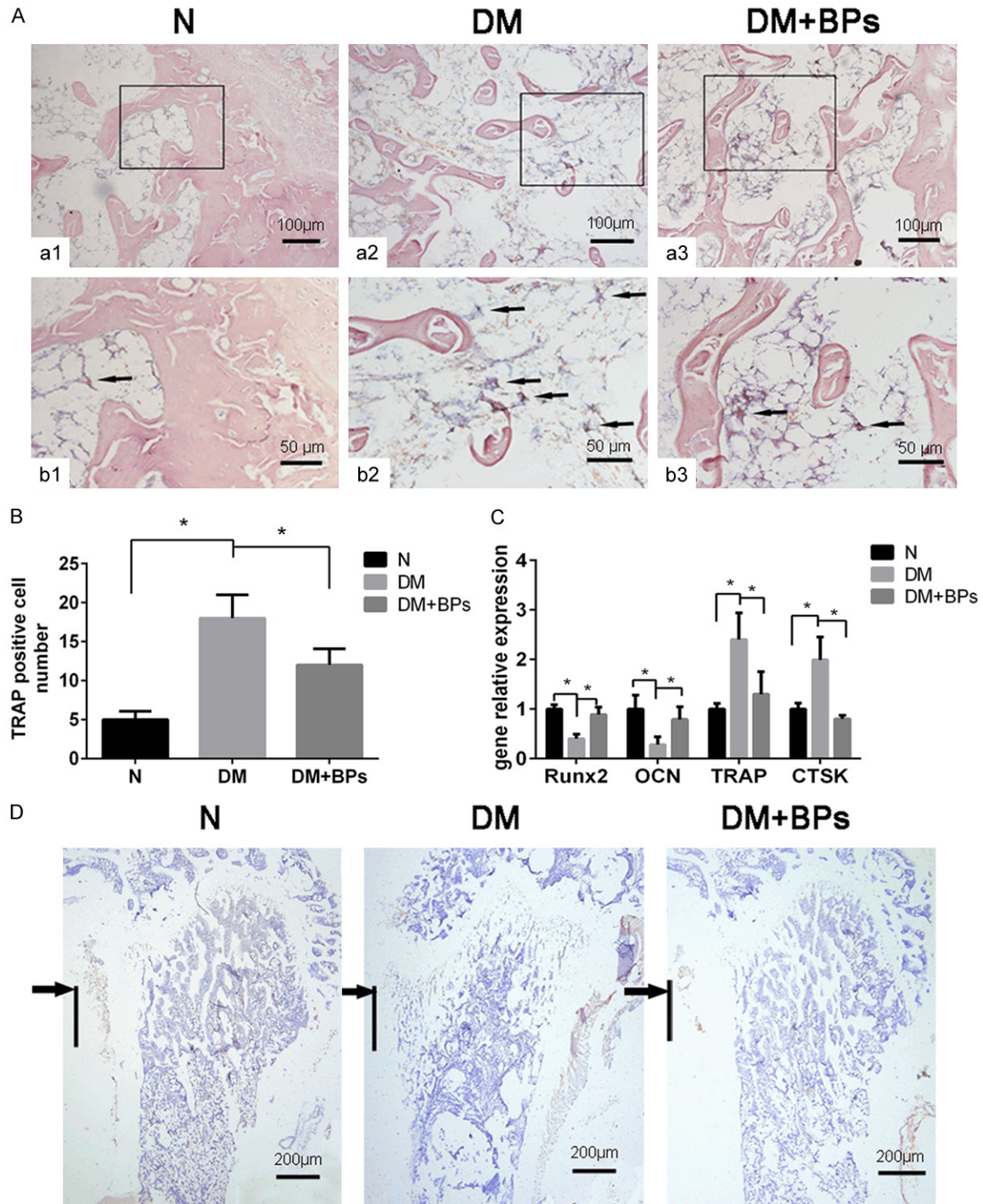
Figure 8. Results of relevant gene expression, histology and immunohistochemistry examinations. (A, a1-a3) TRAP staining of sections derived from the ROI of the femora (original magnification *200). (b1-b3) Higher power fields of the black box areas in (a1-a3) (original magnification *400). (B) The number of *TRAP*-positive multinucleated cells (MNCs) is shown as the mean ± SD (n=3). *P<0.05. (C) Runx2, OCN, TRAP and CTSK expression extracted from the femora of mice. Experiments were performed in at least triplicate. Data are expressed as the mean ± SD (n=3). *P<0.05 (by ANOVA). (D) Immunohistochemistry examinations of OCN. All sections are derived from the ROI of the femora (original magnification *100). The black arrows indicate the segments around the implant. The black line denotes the region of the original implant placement.

tent mesenchymal stem cells, which are expressed in different tissues. Runx2 and

Osterix play critical roles in bone formation by promoting the differentiation of osteoblasts

[61]. The synthesis and secretion of OCN is dependent mainly on mature osteoblasts, which serves as a representation of bone formation [62]. With regard to bone formation, the production of collagen matrix is closely related to OCN, Runx2 and Osterix [63]. Our in vitro study results demonstrated that HG markedly reduced the expression of Runx2, OCN and Osterix in BMSCs. In addition, BPs remarkably promoted cell proliferation compared with HG, particularly the lower concentrations of BPs (10^{-9} mmol/L) ($P<0.05$). In addition, a conspicuous increase in the protein level of Runx2 was observed in the BPs group compared with the HG group, which simultaneously occurred with the upregulation of β-catenin. The Wnt/β-catenin pathways were shown to coincide with the regulation of bone formation, remodeling and metabolism [64, 65] and have been considered main regulators of osteoblastogenesis [66, 67]. Recent research indicated that low-dose BPs facilitated bone formation by promoting osteoblastogenesis and inhibiting apoptosis of osteoblasts [48], while BPs were identified as antiresorptive agents that diminished the function of osteoclasts [68]. Omi H et al [69] demonstrated that low-dose BPs were absorbed rapidly by osteoclasts, improving osteoblast proliferation. To our knowledge, the mechanism of how BPs act on bone remodeling remains unknown. Through our observations, we conclude that the promoted osteoclastic bone resorption and the reduced osteoblastic bone formation were linked to HG conditions, similar to the results demonstrated by Lu H et al.

In conclusion, the results of this study coincide with the hypothesis of the authors that the administration of local BPs to rats with induced diabetic osteoporosis would promote bone reconstruction around implants placed in the femora. It was also demonstrated via the in vitro study that low-dose BPs suppressed osteoclast formation and significantly increased BMSC proliferation. Thus, the results of this study confirm the antiresorptive potential of local application of BPs in lower quality bones to prevent decayed implant osseointegration under T2DM conditions.

Acknowledgements

Disclosure of conflict of interest

None.

Address correspondence to: Leilei Zheng, College of Stomatology, Chongqing Medical University, #426 Northisongshi Rd, Yubei, Chongqing 401147, China. Tel: 15086986968; E-mail: zhengleileicqmu@hospital.cqmu.edu.cn

References

[1] Jackson RD and Mysiw WJ. Insights into the epidemiology of postmenopausal osteoporosis: the women's Health Initiative. Semin Reprod Med 2014; 32: 454-462.

[2] Bonds DE, Larson JC, Schwartz AV, Strotmeyer ES, Robbins J, Rodriguez BL, Johnson KC and Margolis KL. Risk of fracture in women with type 2 diabetes: the women's health initiative observational study. J Clin Endocrinol Metab 2006; 91: 3404-3410.

[3] Kanazawa I, Takeno A, Tanaka KI, Yamane Y and Sugimoto T. Osteoporosis and vertebral fracture are associated with deterioration of activities of daily living and quality of life in patients with type 2 diabetes mellitus. J Bone Miner Metab 2019; 37: 503-511.

[4] Vestergaard P. Discrepancies in bone mineral density and fracture risk in patients with type 1 and type 2 diabetes-a meta-analysis. Osteoporos Int 2007; 18: 427-444.

[5] Chen FP, Kuo SF, Lin YC, Fan CM and Chen JF. Status of bone strength and factors associated with vertebral fracture in postmenopausal women with type 2 diabetes. Menopause 2019; 26: 1-1.

[6] Leslie WD, Morin SN, Lix LM and Majumdar SR. Does diabetes modify the effect of FRAX risk factors for predicting major osteoporotic and hip fracture. Osteoporos Int 2014; 25: 2817-2824.

[7] Baelum V and Ellegaard B. Implant survival in periodontally compromised patients. J Periodontol 2004; 75: 1404-1412.

[8] Cook HP. Immediate reconstruction of the mandible by metallic implant following resection for neoplasm. Ann R Coll Surg Engl 1968; 42: 233-259.

[9] Marchand F, Raskin A, Dionnes-Hornes A, Barry T, Dubois N, Valéro R and Vialettes B. Dental implants and diabetes: conditions for success. Diabetes Metab 2012; 38: 14-19.

[10] Ross RD, Hamilton JL, Wilson BM, Sumner DR and Virdi AS. Pharmacologic augmentation of implant fixation in osteopenic bone. Curr Osteoporos Rep 2014; 12: 55-64.

[11] Abbaspour A, Takata S, Sairyo K, Katoh S, Yukata K and Yasui N. Continuous local infusion of fibroblast growth factor-2 enhances consolidation of the bone segment lengthened by distraction osteogenesis in rabbit experiment. Bone 2008; 42: 98-106.

[12] Hagiwara T and Bell WH. Effect of electrical stimulation on mandibular distraction osteogenesis. J Craniomaxillofac Surg 2000; 28: 12-19.

[13] Ohata T, Maruno H and Ichimura S. Changes over time in callus formation caused by intermittently administering PTH in rabbit distraction osteogenesis models. J Orthop Surg Res 2015; 10: 88.

[14] Fleisch H. Bisphosphonates: mechanisms of action. Endocr Rev 1998; 19: 80-100.

[15] Ruggiero SL, Mehrotra B, Rosenberg TJ and Engroff SL. Osteonecrosis of the jaws associated with the use of bisphosphonates: a review of 63 cases. J Oral Maxillofac Surg 2004; 62: 527-534.

[16] Khan M, Cheung AM and Khan AA. Drug-related adverse events of osteoporosis therapy. Endocrinol Metab Clin North Am 2017; 46: 181-192.

[17] Maraka S and Kennel KA. Bisphosphonates for the prevention and treatment of osteoporosis. BMJ 2015; 351: h3783.

[18] Hilding M and Aspenberg P. Local peroperative treatment with a bisphosphonate improves the fixation of total knee prostheses: a randomized, double-blind radiostereometric study of 50 patients. Acta Orthop 2007; 78: 795-799.

[19] Guimarães MB, Bueno RS, Blaya MB, Shinkai RS and Marques LM. Influence of the local application of sodium alendronate gel on osseointegration of titanium implants. Int J Oral Maxillofac Surg 2015; 44: 1423-1429.

[20] Jakobsen T, Bechtold JE, Søballe K, Jensen T, Greiner S, Vestermark MT and Baas J. Local delivery of zoledronate from a poly (D,L-lactide)-coating increases fixation of press-fit implants. J Orthop Res 2016; 34: 65-71.

[21] Alp YE, Taskaldiran A, Onder ME, Karahan S, Kocyigit ID, Atil F and Tekin U. Effects of local low-dose alendronate injections into the distraction gap on new bone formation and distraction rate on distraction osteogenesis. J Craniofac Surg 2017; 28: 2174.

[22] Dolci LS, Panzavolta S, Torricelli P, Albertini B, Sicuro L, Fini M, Bigi A and Passerini N. Modulation of Alendronate release from a calcium phosphate bone cement: an in vitro osteoblast-osteoclast co-culture study. Int J Pharm 2018; 554: 245-255.

[23] Omi H, Kusumi T, Kijima H and Toh S. Locally administered low-dose alendronate increases bone mineral density during distraction osteogenesis in a rabbit model. J Bone Joint Surg Br 2007; 89: 984-8.

[24] Tekin U, Tüz HH, Onder E, Ozkaynak O, Korkusuz P. Effects of alendronate on rate of distraction in rabbit mandibles. J Oral Maxillofac Surg 2008; 66: 2042-9.

[25] Zheng L, Tu Q, Meng S, Zhang L, Yu L, Song J, Hu Y, Sui L, Zhang J, Dard M, Cheng J, Murray D, Tang Y, Lian JB, Stein GS and Chen J. Runx2/DICER/miRNA pathway in regulating osteogenesis. J Cell Physiol 2017; 232: 182-191.

[26] Schilling T, Küffner R, Klein-Hitpass L, Zimmer R, Jakob F and Schütze N. Microarray analyses of transdifferentiated mesenchymal stem cells. J Cell Biochem 2008; 103: 413-433.

[27] Battaglino R, Kim D, Fu J, Vaage B, Fu XY and Stashenko P. c-myc is required for osteoclast differentiation. J Bone Miner Res 2002; 17: 763-773.

[28] Zheng L, Song J, Li Z, Fan Y, Zhao Z, Chen Y, Deng F and Hu Y. The mechanism of myoblast deformation in response to cyclic strain - a cytomechanical study. Cell Biol Int 2008; 32: 754.

[29] Hu Y, Deng F, Song J, Lin J, Li X, Tang Y, Zhou J, Tang T and Zheng L. Evaluation of miR-29c inhibits endotheliocyte migration and angiogenesis of human endothelial cells by suppressing the insulin like growth factor 1. Am J Transl Res 2015; 7: 866-877.

[30] Bergman K, Engstrand T, Hilborn J, Ossipov D, Piskounova S and Bowden T. Injectable cell-free template for bone-tissue formation. J Biomed Mater Res A 2009; 91: 1111-1118.

[31] Kettenberger U, Ston J, Thein E, Procter P and Pioletti DP. Does locally delivered zoledronate influence peri-implant bone formation? - Spatio-temporal monitoring of bone remodeling in vivo. Biomaterials 2014; 35: 9995-10006.

[32] Kisiel M, Klar AS, Martino MM, Ventura M and Hilborn J. Evaluation of injectable constructs for bone repair with a subperiosteal cranial model in the rat. PLoS One 2013; 8: e71683.

[33] Srinivasan K, Viswanad B, Asrat L, Kaul CL and Ramarao P. Combination of high-fat diet-fed and low-dose streptozotocin-treated rat: a model for type 2 diabetes and pharmacological screening. Pharmacol Res 2005; 52: 313-320.

[34] Dempster DW, Compston JE, Drezner MK, Glorieux FH, Kanis JA, Malluche H, Meunier PJ, Ott SM, Recker RR and Parfitt AM. Standardized nomenclature, symbols, and units for bone histomorphometry: a 2012 update of the report of the ASBMR histomorphometry nomenclature committee. J Bone Miner Res 2013; 28: 2-17.

[35] Wang J, Teng L, Liu Y, Hu W, Chen W, Hu X, Wang Y and Wang D. Studies on the antidiabetic and antinephritic activities of paecilomyces hepiali water extract in diet-streptozotocin-induced diabetic sprague dawley rats. J Diabetes Res 2016; 2016: 4368380.

[36] Janghorbani M, Van Dam RM, Willett WC and Hu FB. Systematic review of type 1 and type 2 diabetes mellitus and risk of fracture. Am J Epidemiol 2007; 166: 495-505.

[37] Di SC, Rubino M, Faggiano A, Vuolo L, Contaldi P, Tafuri N, Tafuto N, Andretti M, Savastano S and Colao A. Spinal deformity index in patients with type 2 diabetes. Endocrine 2013; 43: 651-658.

[38] Carracher AM, Marathe PH and Close KL. International diabetes federation 2017. J Diabetes 2018; 10: 353-356.

[39] Lenzen S. The mechanisms of alloxan- and streptozotocin-induced diabetes. Diabetologia 2008; 51: 216-226.

[40] Min W, Fang P, Huang G, Shi M and Zhang Z. The decline of whole-body glucose metabolism in ovariectomized rats. Exp Gerontol 2018; 113: 106-112.

[41] Alghamdi HS, Bosco R, Both SK, Iafisco M, Leeuwenburgh SC, Jansen JA and van den Beucken JJ. Synergistic effects of bisphosphonate and calcium phosphate nanoparticles on peri-implant bone responses in osteoporotic rats. Biomaterials 2014; 35: 5482-5490.

[42] Giro G, Coelho PG, Pereira RM, Jorgetti V, Marcantonio E and Orrico SR. The effect of oestrogen and alendronate therapies on postmenopausal bone loss around osseointegrated titanium implants. Clin Oral Implants Res 2011; 22: 259-264.

[43] Vohra F, Al-Rifaiy MQ, Almas K and Javed F. Efficacy of systemic bisphosphonate delivery on osseointegration of implants under osteoporotic conditions: lessons from animal studies. Arch Oral Biol 2014; 59: 912-920.

[44] Pura JA, Bobyn JD and Tanzer M. Implant-delivered alendronate causes a dose-dependent response on net bone formation around porous titanium implants in canines. Clin Orthop Relat Res 2016; 474: 1224-1233.

[45] Mathijssen NM, Buma P and Hannink G. Combining bisphosphonates with allograft bone for implant fixation. Cell Tissue Bank 2014; 15: 329-336.

[46] Miettinen SS, Jaatinen J, Pelttari A, Lappalainen R, Mönkkönen J, Venesmaa PK and Kröger HP. Effect of locally administered zoledronic acid on injury-induced intramembranous bone regeneration and osseointegration of a titanium implant in rats. J Orthop Sci 2009; 14: 431-436.

[47] Cuairán C, Campbell PM, Kontogiorgos E, Taylor RW, Melo AC and Buschang PH. Local application of zoledronate enhances miniscrew implant stability in dogs. Am J Orthod Dentofacial Orthop 2014; 145: 737-749.

[48] Ye T, Cao P, Qi J, Zhou Q, Rao DS and Qiu S. Protective effect of low-dose risedronate against osteocyte apoptosis and bone loss in ovariectomized rats. PLoS One 2017; 12: e0186012.

[49] Guimarães MB, Bueno RS, Blaya MB, Hirakata LM and Hübler R. Diphosphonate immobilization on hydroxyapatite-coated titanium--method description. Implant Dent 2013; 22: 356-359.

[50] Jakobsen T, Baas J, Bechtold JE, Elmengaard B and Søballe K. Soaking morselized allograft in bisphosphonate can impair implant fixation. Clin Orthop Relat Res 2007; 463: 195-201.

[51] Virdi AS, Irish J, Sena K, Liu M, Ke HZ, Mcnulty MA and Sumner DR. Sclerostin antibody treatment improves implant fixation in a model of severe osteoporosis. J Bone Joint Surg Am 2015; 97: 133-40.

[52] Brunetti G, D'Amato G, Chiarito M, Tullo A, Colaianni G, Colucci S, Grano M and Faienza MF. An update on the role of RANKL-RANK/osteoprotegerin and WNT-ß-catenin signaling pathways in pediatric diseases. World J Pediatr 2019; 15: 4-11.

[53] Xiong Y, Yang HJ, Feng J, Shi ZL and Wu LD. Effects of alendronate on the proliferation and osteogenic differentiation of MG-63 cells. J Int Med Res 2009; 37: 407-416.

[54] Massey HM and Flanagan AM. Human osteoclasts derive from CD14-positive monocytes. Br J Haematol 1999; 106: 167-170.

[55] Boyle WJ, Simonet WS and Lacey DL. Osteoclast diVerentiation and activation. Nature 2003; 423: 337-42.

[56] Battaglino R, Kim D, Fu J, Vaage B, Fu X and Stashenko P. c-myc is required for osteoclast differentiation. J Bone Miner Res 2002; 17: 763-73.

[57] Russell RG, Watts NB, Ebetino FH and Rogers MJ. Mechanisms of action of bisphosphonates: similarities and differences and their potential influence on clinical efficacy. Osteoporos Int 2008; 19: 733-759.

[58] Idris AI, Rojas J, Greig IR, Van't Hof RJ, Ralston SH. Aminobisphosphonates cause osteoblast

apoptosis and inhibit bone nodule formation in vitro. Calcif Tissue Int 2008; 82: 191-201.

[59] Lu H, Kraut D, Gerstenfeld LC and Graves DT. Diabetes interferes with the bone formation by affecting the expression of transcription factors that regulate osteoblast differentiation. Endocrinology 2003; 144: 346-352.

[60] Orriss IR, Key ML, Colston KW and Arnett TR. Inhibition of osteoblast function in vitro by aminobisphosphonates. J Cell Biochem 2009; 106: 109-118.

[61] Li M, Wu P, Shao J, Ke Z, Li D and Wu J. Losartan inhibits vascular calcification by suppressing the BMP2 and Runx2 expression in rats in vivo. Cardiovasc Toxicol 2016; 16: 172.

[62] Ducy P, Desbois C, Boyce B, Pinero G, Story B, Dunstan C, Smith E, Bonadio J, Goldstein S and Gundberg C. Increased bone formation in osteocalcin-deficient mice. Nature 1996; 382: 448-452.

[63] Bandeira F, Costa AG, Soares Filho MA, Pimentel L, Lima L and Bilezikian JP. Bone markers and osteoporosis therapy. Arq Bras Endocrinol Metabol 2014; 58: 504-513.

[64] Bodine PVN, Robinson JA, Bhat RA, Billiard J, Bex FJ and Komm BS. The role of Wnt signaling in bone and mineral metabolism. Clinical Reviews in Bone and Mineral Metabolism 2006; 4: 73-96.

[65] Reinhold MI and Naski MC. Direct interactions of Runx2 and canonical Wnt signaling induce FGF18. J Biol Chem 2007; 282: 3653.

[66] Lerner UH and Ohlsson C. The WNT system: background and its role in bone. J Intern Med 2015; 277: 630-649.

[67] Milat F and Ng KW. Is Wnt signalling the final common pathway leading to bone formation. Mol Cell Endocrinol 2009; 310: 52-62.

[68] Bellido T and Plotkin LI. Novel actions of bisphosphonates in bone: preservation of osteoblast and osteocyte viability. Bone 2011; 49: 50-55.

[69] Omi H, Kusumi T, Kijima H and Toh S. Locally administered low-dose alendronate increases bone mineral density during distraction osteogenesis in a rabbit model. J Bone Joint Surg Br 2007; 89: 984-8.